Journal of Materials Chemistry C

ROYAL SOCIETY OF CHEMISTRY

PAPER

View Article Online
View Journal | View Issue

Cite this: J. Mater. Chem. C, 2023, 11, 1435

Mesogenic $[Rh(L)_4](A)$ complexes form mesophases with $Rh^I\cdots Rh^I$-containing and triphenylene-discotic segregated columns. Effect of $Rh^I\cdots Rh^I$ interactions and $A^- = [Au(CN)_2]^-$ on hole mobility†

Verónica Conejo-Rodríguez, [a] Bertrand Donnio, *[b] Benoît Heinrich, [b] Roberto Termine, [c] Attilio Golemme [c] and Pablo Espinet *[a]

Received 31st May 2022,
Accepted 22nd December 2022

DOI: 10.1039/d2tc02272a

rsc.li/materials-c

Rh^I complexes $[Rh(\mathbf{L})_4](A)$ ($A^- = Cl^-$, BF_4^-, $[Au(CN)_2]^-$) with conventional arylisocyanides (*p*-$MeC_6H_4(NC)$, $\mathbf{L^A}$; *p*-$MeOC_6H_4(NC)$, $\mathbf{L^B}$; 3,5-$(OMe)_2C_6H_3(NC)$, $\mathbf{L^C}$) or with the alkoxy-functionalized triphenylene-arylisocyanides $TPh(OC_{12}H_{25})_5(O(CH_2)_6OC_6H_4(NC)$-*p*) ($\mathbf{L^{D1}}$) and $TPh(OC_{12}H_{25})_5(O(CH_2)_6OC_6H_2Me_2(NC)$-*p*) ($\mathbf{L^{D2}}$), have been prepared and their self-assembly, aggregation, optical, redox, mesogenic and conducting properties investigated. Intermolecular π–π stacking, $Rh^I\cdots Rh^I$, and $Rh^I\cdots Au^I$ interactions rule the crystal packing and aggregation in solution for the complexes with $\mathbf{L^A}$, $\mathbf{L^B}$, and $\mathbf{L^C}$. For the Rh^I complexes with the alkoxy-functionalized-triphenylene isocyanides $\mathbf{L^{D1}}$ and $\mathbf{L^{D2}}$ mesogenic behaviour is induced, giving rise to multicolumnar mesophases in broad temperature ranges (*ca.* 70–160 °C). Detailed analysis (POM, DSC, SAXS/WAXS and GIWAXS) of the columnar mesophases has allowed us to propose precise packing models that explain the diverse supramolecular arrangements found in the nanostructured condensed phases. Columnar alignments predominantly with Rh···Rh interactions (or Rh···Au, only for $\mathbf{L^{D2}}$ in specific conditions) are observed, depending on the aligning conditions. The hole mobility in the columnar mesophases of the complexes with Rh···Rh interactions are ~1 $cm^2\ V^{-1}\ s^{-1}$, that is up to four orders of magnitude higher than those reported for columnar mesophases of organic triphenylene derivatives, and increases one order of magnitude further in the mesophases containing the $[Au(CN)_2]^-$ counteranion.

Introduction

Stable d^8 square-planar rhodium(I) complexes $[Rh(CNAr)_4](A)$ (Ar = aryl; A^- = anion) have been reported since early studies in the 1970s.[1] Many of them show a natural tendency to establish homometallic interactions forming $[Rh(CNAr)_4]_n^{n+}$ oligomers (n = 1, 2, 3…) in the solid state and in concentrated solutions, in spite of the repulsive contribution of identical positive charges. Stabilizing π–π interactions overcome this electrostatic repulsion and give rise to Rh···Rh orbital interactions at distances significantly shorter than the sum of van der Waals radii. These Rh···Rh orbital interactions have a relatively small contribution to the stability of these polynuclear complexes compared to the π–π interactions (about 10–15% of the total stabilizing forces),[2] but they are responsible for their remarkable photophysical properties.[3] The appropriate combination of metal–metal interactions with other (donor–acceptor, hydrophobic–hydrophilic, cation–anion) attractive interactions facilitates the design of a vast range of functional nanomaterials such as sensors, nanowires, and ionic liquids.[1,3b–6]

For a different reason, $(Q)[Au(CN)_2]$ (Q^+ = cation) d^{10} complexes also give rise to oligomeric complexes with Au···Au interactions. In this case, where aryls are absent, it is the aurophilic interactions that help to overcome the electrostatic repulsion between the $[Au(CN)_2]^-$ anions.[7,8] Speaking in general, there is a multitude of studies of luminescent materials based on the presence of Au···Au aurophilic interactions, including our

[a] IU CINQUIMA/Química Inorgánica, Facultad de Ciencias, Universidad de Valladolid, E-47071 Valladolid, Spain. E-mail: espinet@qi.uva.es
[b] Institut de Physique et Chimie des Matériaux de Strasbourg (IPCMS), UMR 7504 (CNRS-Université de Strasbourg), F-67034 Strasbourg Cedex 2, France. E-mail: bertrand.donnio@ipcms.unistra.fr
[c] LASCAMM CR-INSTM, CNR-Nanotec, Dipartimento di Fisica, 87036 Rende, Italy

† Electronic supplementary information (ESI) available: Synthesis and chemical characterisation details, UV-Visible and electrochemical data, POM, DSC SAXS/WAXS and GIWAXS and hole mobility studies on the mesophases. CCDC 2091366 and 2091367. For ESI and crystallographic data in CIF or other electronic format see DOI: https://doi.org/10.1039/d2tc02272a

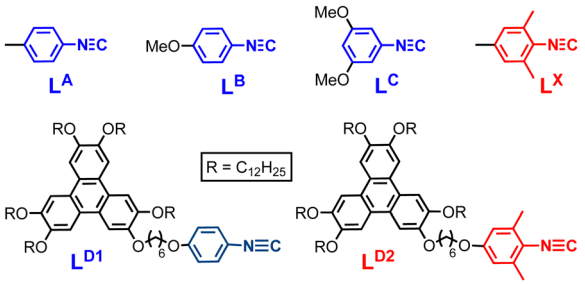

Chart 1 Arylisocyanide ($L^{A,B,C,X}$) and TPhisocyanide (L^{D1} and L^{D2}) ligands used in this work. In the following we keep red colour to highlight the 2,6-Me_2 substituted isocyanides.

recent report of gold complexes that are non-luminescent solid materials but give rise to luminescent mesophases upon melting or grinding the solid.[9]

Surprisingly, the synthetic possibility of combining $[Au(CN)_2]^-$ and $[Rh(CNAr)_4]^+$ complexes in molecular systems, which might facilitate the formation of compounds with Rh···Au interactions by cation–anion electrostatic attraction, had apparently been disregarded. Our group recently published a mixed $[Rh(CNXylyl)_4][Au(CN)_2]$ system, in which the contribution of the anion–cation attractive forces between d^8 $[Rh(CNXylyl)_4]^+$ and d^{10} $[Au(CN)_2]^-$ gives rise, in the solid state, to different crystals (sometimes different polymorphs) displaying $d^8\cdots d^{10}$ short distances. The casual choice of the commercial CNXylyl (L^X, Chart 1) as ligand was fortunate because the presence of two *ortho* Me groups in this isocyanide induces some reluctance to the formation of the multiple intra-unit π–π stackings observed in other $[Rh(CNAr)_4]^+$ cationic complexes and leads instead to the formation of polymetallic arrangements where Rh···Au interactions are preferred (Fig. 1).[10] This interesting and rich solid state behaviour has prompted us to explore further these two metallic systems and their binary combination in the design of metal-containing thermotropic liquid crystals (metallomesogens).[11,12] The tendency of both metal centres to create M···M interactions in concentrated solutions and in the solid state looks promising for building potentially semiconductor columnar mesophases with separate channels for the transport of charges, holes or electrons. We have chosen the triphenylene unit (TPh), functionalized with lateral aliphatic chains (one bringing a TPhisocyanide) as a powerful inductor of columnar mesophases.

Triphenylene offers many possibilities of functionalization around its core. This has yielded a wide variety of materials self-assembling into many types of columnar mesophases,[13–16] and having different applications in several fields.[13,17–19] Compared to the many reports of TPh organic liquid crystals, studies on metallomesogens containing triphenylene derivatives are scarce.[20–22] In the last years we have published a few studies on several liquid crystals using metalorganic complexes and triphenylene systems of different typologies,[23] none utilizing Rh, and all structurally very diverse from the ones reported here.

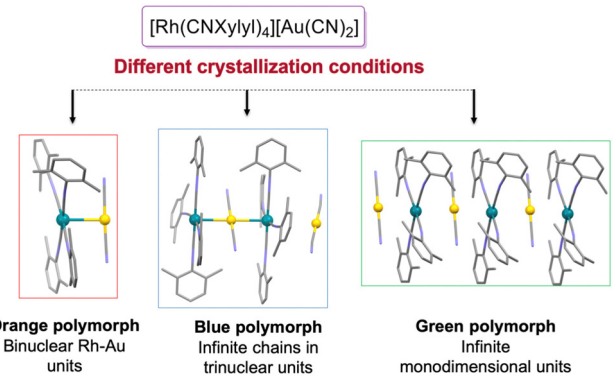

Fig. 1 Examples of different crystal polymorphs of $[Rh(CNXylyl)_4]$-$[Au(CN)_2]$ with Rh···Au interactions.[10]

Results and discussion

Synthesis and characterization of the arylisocyanide ligands

In this work we pursue the synthesis of Rh^I columnar metallomesogens $[Rh(L)_4](A)$ (A^- = Cl^-, BF_4^-; L = aryl isocyanide) with Rh···Rh interactions as potentially flexible monodimensional conductors. We use the triphenylene moiety (TPh) to support the aryl isocyanide moiety that has to coordinate to Rh. Three conventional arylisocyanide ligands with no substituent at the *ortho* position, $L^{A–C}$, are used as simpler models of the triphenyleneisocyanide ligand L^{D1} (Chart 1), to obtain information on self-assembling of Rh centres. Similarly, L^X is a model of the TPh isocyanide L^{D2}.

According to our previous solid state results with L^X (Fig. 2),[10] for A^- = $[Au(CN)_2]^-$, Rh···Au interactions in the mesophase might be more likely to appear with L^{D2} (as with L^x in the solid) than with L^{D1}.

The arylisocyanide and TPhisocyanide syntheses used modified literature methods.[8a,23d,24] The previously unreported TPhisocyanide ligand **6** (L^{D2}) was synthesized as shown in Scheme 1. See ESI† for NMR and IR data and comments (Table S1 and Fig. S4–S11, ESI†).

Synthesis and characterization of $[Rh(L)_4](A)$ model-aryl and mesogenic-tPhisocyanide complexes.

As summarized in Scheme 2, the reaction of 8 equivalents of ligands L^A–L^{D1} with $[RhCl(COD)]_2$ (COD = 1,5-cyclooctadiene) in

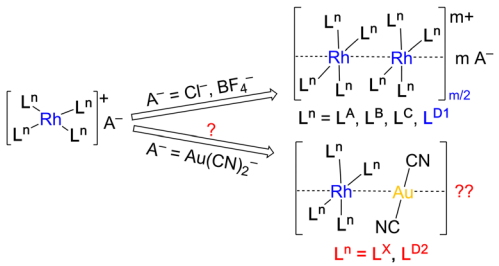

Fig. 2 Possible M···M interactions in the solid or, eventually, in mesophases of complexes with promesogenic L^{D1} and L^{D2}.

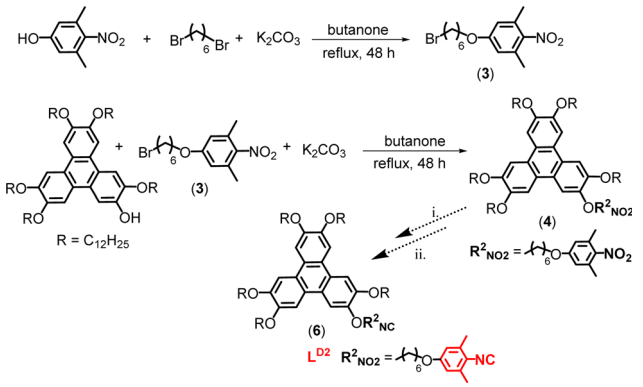

Scheme 1 Synthesis of $\mathbf{L^{D2}}$: (i) Sn, formic acid, toluene, reflux 3 h; (ii) triphosgene, Et_3N, dry CH_2Cl_2, 0–25 °C. See ESI† for details.

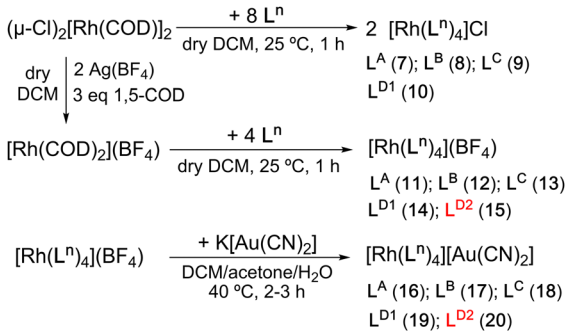

Scheme 2 Synthetic pathways to [RhL4](A) complexes from precursors $(\mu\text{-Cl})_2[Rh(COD)]_2$ and $[Rh(COD)_2](BF_4)$.

dichloromethane led, as reported for related systems,[1d,3b–6] to the corresponding $[Rh(\mathbf{L})_4](Cl)$ complexes **7–10**. Complexes $[Rh(\mathbf{L})_4](BF_4)$ (**11–15**) were synthesized from $[Rh(COD)_2](BF_4)$ and 4 equivalents of the corresponding isocyanide. Finally the heterobimetallic complexes $[Rh(\mathbf{L})_4][Au(CN)_2]$ (**16–20**) were obtained by anion metathesis of the BF_4 complexes with $(K)[Au(CN)_2]$. The complex with $\mathbf{L^X}$ has been reported previously.[25]

For complexes with $\mathbf{L^{D2}}$, an equilibrium mixture of $[RhCl(\mathbf{L^{D2}})_3]$ and $[Rh(\mathbf{L^{D2}})_4](Cl)$ was formed. This had been observed previously for the xylylisocyanide ligand $\mathbf{L^X}$,[1d] but in the case of $\mathbf{L^{D2}}$ the problem could not be solved using an excess of $\mathbf{L^{D2}}$ to displace the equilibrium, as we did for $\mathbf{L^X}$, because the mixture of excess ligand and complex $[Rh(\mathbf{L^{D2}})_4](Cl)$ could not be separated.

Solid-state characterization of arylisocyanide complexes

Attempts at growing single crystals suitable for X-ray diffraction provided some solid-state structures of the model complexes. Deep-blue single crystals of $[Rh(\mathbf{L^C})_4](Cl)$ (**9**), obtained by slow diffusion of hexane into a diluted solution in CH_2Cl_2 of the blue solid obtained in the synthesis, provided the X-ray diffraction structure depicted in Fig. 3, showing a polymeric arrangement of the Rh atoms at distance Rh···Rh = 3.898 Å. In these polymeric structures the anions are located somewhere close

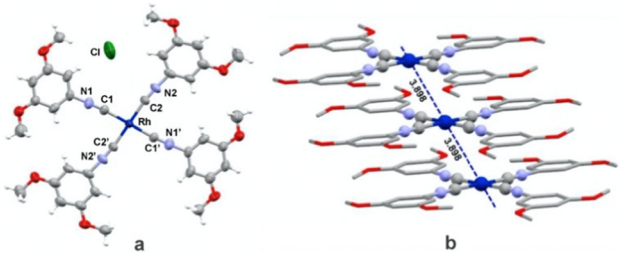

Fig. 3 (a) Crystal structure of blue crystals of $[Rh(\mathbf{L^C})_4](Cl)$ (**9**). Most prominent distances (Å) and angles: Rh(1)–C(1) = 1.943(9); Rh(1)–C(2) = 1.970(8); C(1)-N(1) = 1.157(11); C(2)-N(2) = 1.134(10); C(1)-Rh(1)–C(2) = 92.8(4); C(2)-Rh(1)–C(3) = 87.2(4); (b) Crystal packaging: infinite chains of $[Rh\{CNC_6H_3(OMe)_2\text{-}3,5\}_4]Cl$ (**9**), with Rh···Rh = 3.898 Å.

to the external zone of the aryls, as shown for the chloride of **9** in Fig. 3a.

In the case of $[Rh(\mathbf{L^A})_4](BF_4)$ (**11**), deep-red crystals were obtained by slow diffusion of hexane into a diluted solution in acetone of the green solid isolated in the synthesis. A dimeric arrangement of cations, with Rh···Rh = 3.473 Å was found (Fig. 4).

The deep colours of the blue crystals of $[Rh(\mathbf{L^C})_4](Cl)$ (**9**) and the red crystals of $[Rh(\mathbf{L^A})_4](BF_4)$ (**11**) are typical of Rh complexes that display strong π–π stacking interactions, which force Rh to Rh approximation and induce $Rh^I\cdots Rh^I$ non-covalent interactions (NCI),[26] also observed in other similar deeply coloured Rh^I complexes, at relatively short distances that are shorter than the sum of van der Waals radii (2 × 2.44 = 4.88 Å),[27] but much larger than the sum of covalent radii (2 × 1.42 = 2.84 Å).[28] These $Rh^I\cdots Rh^I$ interactions in Rh^I oligomers or polymers can display colours in the red-to-blue range. The aryl π–π stacking and the possible aryl substituents, on the side of the ligand, and the Rh···Rh distances, on the side of the metal, affect the LUMO and, respectively, HOMO energies of complexes and the colours observed. For instance, **11**, a dimer with good π–π stacking (short Rh···Rh distance = 3.473 Å) is red, but the analogous dimers $[Rh_2\{(p\text{-}CNC_6H_4F)_4\}_2]Cl_2\cdot(OH_2)_2$ (Rh···Rh = 3.207 Å and $[Rh_2\{(p\text{-}CNC_6H_4(NO_2))_4\}_2]Cl_2$

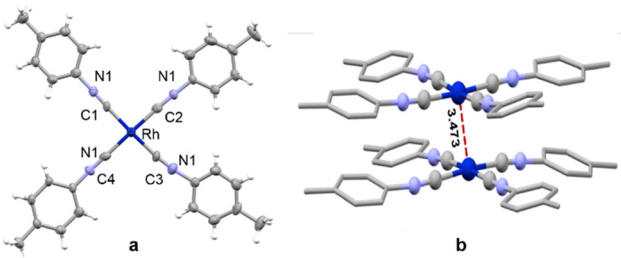

Fig. 4 (a) Crystal structure of red crystals of $[Rh(L^A)_4](BF_4)$. (11). BF_4 was omitted to simplify the figure. Most prominent distances (Å) and angles: Rh(1)–C(1) = 1.963(7); Rh(1)–C(2) = 1.967(9); Rh(1)–C(3) = 1.940(8); Rh(1)–C(4) = 1.964(9); C(1)-N(1) = 118(9); C(2)-N(2) = 1.182(10); C(3)-N(3) = 1.147(10); C(4)-N(4) = 1.166(10); C(1)-Rh(1)–C(2) = 91.0(3); C(2)-Rh(1)–C(3) = 86.4(3); C(3)-Rh(1)–C(4) = 92.8(3); C(4)-Rh(1)–C(1) = 89.6(3); C(1)-Rh(1)–C(3) = 174.4(3); C(2)-Rh(1)–C(4) = 177.3(3); (b) Crystalline packaging: dimers of $[Rh(L^A)_4](BF_4)$.

(Rh···Rh = 3.25 Å are blue and deep green, respectively.[1e] Clearly, in these cases the colour switch is due to the change of *p*-substituent (Me gives red but the electron withdrawing F and NO_2 substituents give green–blue). The structurally different crystals of the polymeric complex **9**, with 3,5-OMe substituents and a less efficient packing (Rh···Rh = 3.898 Å) are also deep blue. Note also that polymers, having the aryl π electron density involved in double π–π stacking, lead to longer Rh···Rh distances than the dimers. For electronically similar substituents (H, Me) the colour could be expected to be mainly a function of the structure, that is, of the efficiency of the stacking and, consequently, of the Rh···Rh distances.

Y. Yamamoto *et al.* estimated the spatial requirements of some 2,6-substituents in structures of rhodium complexes with phenyl isocyanides.[1d] They used values of the ''wideness angle'' and the ''thickness angle'', defined by the tangents from the Rh atom centre to the atoms marking the molecular frontiers of the substituted aryls in the plane and in the C_{ipso} direction. These angles are 77° and 48° for TPhNC *versus* 106° and 53° for 2,6-Me-C_6H_4NC. The bulkiness of the isocyanides, as estimated by these angles, can impose the necessity for the isocyanide aryls to adopt smaller or larger twists relative to the RhC_4 coordination plane. Small twists will be compatible with good π–π stacking and short Rh···Rh distances in dimers. Large twists weaken the strength of the π–π stacking and bring to longer Rh···Rh distances but are compatible with polymeric structures or, in the limit, to formation of monomers, as in the case of the yellow complex $[Rh(CNXylyl)_4](BF_4)$,[10] whose X-ray diffraction structure consists of monomeric cation units, with no π–π stacking and no Rh···Rh interactions.

Our main interest in this work is centred on the triphenylene isocyanide complexes with $\mathbf{L^{D1}}$ or $\mathbf{L^{D2}}$ (Scheme 2 : **10**, **14**, **15**, **19**, **20**). Their solid state or their potential mesomorphic structures should be conditioned by the two moieties prone to columnar π–π stacking, namely the TPh groups and the aryls of the $[RhL_4]$ groups. The 2,6-Me substituted $\mathbf{L^{D2}}$ complexes can be hypothesized to be less efficient for π–π stacking than those with $\mathbf{L^{D1}}$. Unfortunately, due to the presence of long alkoxylic chains, suitable single crystals of them by X-ray diffraction to ascertain this hypothesis could not be obtained but, considering the fairly similar electronegativity of the 2,6- aryl substituents of $\mathbf{L^{D1}}$ or $\mathbf{L^{D2}}$ (H and Me, respectively), it is not unreasonable to take the colours of their analogous complexes as indicative of structural similarity difference in aryl π–π stacking in their solid-state.

The pristine solids of the three $[Rh(\mathbf{L^{D1}})_4]^+$ complexes (Cl^-, BF_4^- or $[Au(CN)_2]^-$ as anion) are deep green, a typical colour of complexes with polymeric Rh···Rh interactions (*e.g.* **9**). In contrast, the two complexes with ligand $\mathbf{L^{D2}}$ (BF_4^- or $[Au(CN)_2]^-$ as anion, the other could not be isolated) are orange–red–brownish solids, suggesting that the 2,6-Me substituted TPhisocyanides might hampering an efficient polymeric π–π stacking of $[Rh(\mathbf{L^{D2}})_4]^+$ cations forcing a structural change perhaps in favour of dimers (e.g **11**). This plausible interpretation finds some support later on, in the mesogenic studies.

Thermal and mesomorphic behaviour

The mesophases of the complexes are extremely viscous. Because of this, the phase transitions are very slow and the DSC studies show transition curves spanning over 20–30 °C at the base (*e.g.* Fig. S50, ESI†), with little variation with the heating/cooling rate. Consistent with the DSC curves, optical observations suggest unusually large coexistence of the two mesophases involved in the transition. In the POM studies the samples need to be pressed and sheared under the cover glass, in order to help for formation of homogeneous mesophases, against the inertia retarding the phase transitions. Due to this difficulty, the transition temperatures, assigned by DSC, should be considered with some range of uncertainty.

The thermal and thermodynamic data are gathered in Table 1 and geometrical data of the mesophases are collected later in Table. S4 (ESI†). Neither $\mathbf{L^{D1}}$ nor $\mathbf{L^{D2}}$ are mesomorphic, but a rich mesomorphism was induced in their Rh^I complexes, which display good thermal stability in the range of study. The data in Table 1 correspond to the second heating. Upon cooling after the first heating, compounds **14**, **15**, **19** and **20** do not revert to the crystalline phase obtained from the solution, but to a glass phase. For this reason, their second heatings start at lower temperatures and generate mesophases below 0 °C, roughly reproducing the first cooling cycle.

Selected pictures of mesophases under crossed polarizers are given in ESI.† However, the changes in colour, which are

Table 1 Thermal and thermodynamic data of $[Rh(\mathbf{L^{D1}})_4](A)$ and $[Rh(\mathbf{L^{D2}})_4](A)$ compounds

Comp.	Transition[a]	T °C[b]	ΔC_p[b] (J per g °C)	ΔH[b] (kJ mol^{-1})
$\mathbf{L^{D1}}$ (ref. 23*b*)	Cr → I	49		81.6
$\mathbf{L^{D2}}$, **6**	Cr → Cr_1	46.3	—	56.54
	Cr_1 → Cr_2	52.7	—	5.08
	Cr_2 → I	58.5	—	2.12
$[Rh(\mathbf{L^{D1}})_4](A)$				
10 A = Cl	PCr → $Col_{o/r}$[c]	−3.3	—	93.15
	$Col_{o/r}$[c] → Col_r	49.5	—	1.46
	Col_r → I	91.7	—	18.86
14 A = BF_4	g→ $Col_{o/r}$[c]	−9.4	0.70	—
	$Col_{o/r}$[c] → Orth	137.5	—	1.15
	Orth → I	154.2	—	15.83
19 A = $[Au(CN)_2]$	g → $Col_{o/r}$[c]	−7.9	0.25	—
	Col_{r1} → Col_{r2}	34.0	—	46.05
	Col_{r2} → I	169.2	—	32.50
$[Rh(\mathbf{L^{D2}})_4](A)$				
15 A = BF_4	g → Amo_{Col}	−8.2	0.39	—
	Amo_{Col} → Col_o	43.39	—	44.3[d]
	Col_o → I	79.0	—	44.10
20A = $[Au(CN)_2]$	g → Amo_{Col}	−5.0	0.35	—
	Amo_{Col} → Col_o	35.1	—	26.53
	Col_o → I	89.7[d]	—	49.18

[a] Cr, Cr_1, Cr_2 and PCr: Crystalline and poorly developed crystalline phases; g: glass, Amo_{Col}: Amorphous superlattice-like order in the solid state with local-range oblique symmetry; Col_r (Col_{r1} and Col_{r2}): Rectangular columnar mesophase; Col_o: Oblique columnar mesophase; Orth: Orthorhombic mesophase; I: Isotropic Liquid. [b] Transition onset temperatures, data from second heating). Heating and cooling at 10 °C/min. Ovl. = overlapped. [c] Col_o at 20 °C from thin-film and Col_r at 20 °C from bulk. [d] Overlapped.

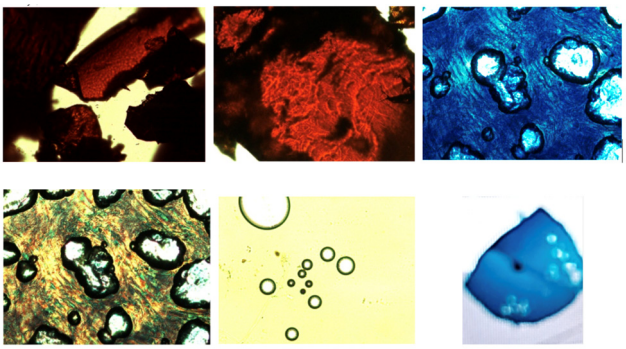

Fig. 5 First heating of $[Rh(\mathbf{L^{D2}})_4](BF_4)$ (**15**), as seen without polarizers for better colour observation.

indicative of structural changes, and the coexistence of phases is much better observed without polarization. The pictures in Fig. 5 correspond to this kind of observation and are for the first heating evolution of complex **15**.

Complex **15** is red–orange in the waxy solid (picture upper row-left, 20 °C). Upon heating, it first melts slowly (picture upper row-centre, 30 °C) to a red mesophase compatible to stacking of dimers. Then it changes slowly to a deep blue mesophase, which is neatly observed in the next picture (upper row-right, 70 °C). This colour suggests a structural change in this transition to a polymeric stacking. When the temperature reaches the clearing point, the material gains fluidity and some apparently green evanescent microdomains appear (picture in down row-left, 80 °C), which eventually clear to a light-yellow fluid isotropic liquid (down-centre, 95 °C). As a reference, lacking of Rh···Rh interactions in the solid state, the yellow $[Rh(CNXylyl)_4](BPh_4)$ is monomeric.[4] The blue colour is recovered upon cooling to give finally a blue glass phase. The down-right picture (taken out of the microscope, a bit out of focus) is the sample studied in this series of pictures, on its glass support, at 20 °C). The structural change to blue is irreversible and the initial red–orange colour is never thermally recovered.

Another interesting observation when comparing complexes $[(Rh(\mathbf{L^{D1}})_4](A)$ and $[(Rh(\mathbf{L^{D2}})_4](A)$ (A = BF_4, $[Au(CN)_2]$) is the huge difference in mesophase range and in clearing point of homologous complexes with $\mathbf{L^{D1}}$ *vs.* $\mathbf{L^{D2}}$ (Table 1, compound **14** *vs.* **19** and **15** *vs.* **20**). This is due to the apparently small change (H for Me) of the 2-6-substituents in the TPhlisocyanide moiety in molecules that contain in addition one triphenylene and six long alkoxylic chains per isocyanide. This supports that the main interactions conditioning the melting and clearing points are again those between the $[Rh(TPhisocyanide)_4]^+$ fragments discussed for the solid state.[1d] In fact, the melting points to the isotropic liquid of the free ligands (non-mesogenic) are 58.5 °C for $\mathbf{L^{D2}}$ and only 49 °C for $\mathbf{L^{D1}}$ (lower for $\mathbf{L^{D1}}$), but the clearing points of the $\mathbf{L^{D1}}$ complexes (154.2 for **14** and 169.2 °C for **19**) are *ca.* 70 °C higher than for the analogous $\mathbf{L^{D2}}$ complexes (79.0 °C for **15** and 89.7 °C for **20**). Although it might be expected that the columnar interactions between TPh disks is a strong support of the framework of segregated TPh and $Rh^I\cdots Rh^I$ columns mesophases observed, the clearing points reveal that the arylisocyanide π–π interactions at rhodium, stronger with $\mathbf{L^{D1}}$ or weaker with $\mathbf{L^{D2}}$, are in both cases decisive for the stability of the whole columnar structure. When these π–π interactions are stronger ($\mathbf{L^{D1}}$), the system can sustain heating to 154.2 and 169.2 °C, but when they are weaker ($\mathbf{L^{D2}}$) due to the disturbing effect of the Me substituents on aryl packing,[1d] the whole elaborate scaffolding collapses at 79.0 or 89.7 °C. In other words, the π–π interactions of the isocyanide aryls (aryl:TPh = 1 : 1) are the main enthalpic contribution to mesophase stability, but only the cooperation of the two types of column (TPh:Rh = 4 : 1, analysed immediately in the SAXS/WAXS and GIWAXS section) compensates the unfavourable entropic contribution of this self-association and keeps the columnar arrangement layout. For a discussion and examples on the enthalpy/entropy effects in the formation of columnar mesophases, see ref. 23*d*.

Overall, the different colours observed in the solid state and the mesophases can be understood as follows: compounds **14** and **19**, green in the solid state and blue in the mesophase, may have polymeric Rh···Rh interactions, as in model complex **9**, associated to relatively long Rh···Rh distances in both states. In contrast, compounds **15** and **20** could have, in the solid state, monomeric or dimeric structures (as the dimeric red complex **11**) and then undergo, at higher temperature, a structural change to polymeric Rh···Rh interactions at long Rh···Rh distances that allow to accommodate a small tilting of the 2,6-Me_2 aryls. The high viscosity of **15** and **20** at room temperature makes this red to blue change irreversible upon cooling.

SAXS/WAXS and GIWAXS studies.

SAXS/WAXS studies can provide much information about the self-assembling organization of the different phases but almost none about the existence of Rh···Rh interactions. However, the characteristic colours observed in the mesophases (*e.g.* Fig. 5) can be taken as qualitative support of their existence. SAXS/WAXS studies confirm that the five complexes (Table S4, ESI†) self-organize into multi-segregated structures. As anticipated, distinct self-assembled bundles of organometallic cores between piles of stacked triphenylene mesogens, separated from each other by the aliphatic continuum (chains and spacers), are found. All the data of the mesophases obtained from SAXS/WAXS are summarized in Table S3 (ESI†), and the X-ray patterns are shown in Fig. 6, 7 and Fig. S42–S47 (ESI†).

The presence of only broad signals over the entire X-ray angular domain considered indicates that the pristine solid-state structures are initially only defined at local range, involving few neighbouring molecules. Specifically, the patterns contain two broad small-angle peaks with maximum at D_1 = 50 ± 1 Å and D_2 = 20.5 ± 0.5 Å, which are attributed to the average lateral distances separating RhA domains and TPh domains, respectively. For D_1, the correlation length calculated from Scherrer equation with shape factor K = 0.9 is ξ_1 = 12 nm for $[Rh(\mathbf{L^{D1}})_4]Cl$, 17 nm for $[Rh(\mathbf{L^{D1}})_4](BF_4)$, 28 nm for $[Rh(\mathbf{L^{D1}})_4]$-$[Au(CN)_2]$, and 13 nm for $[Rh(\mathbf{L^{D2}})_4](BF_4)$ and $[Rh(\mathbf{L^{D2}})_4][Au(CN)_2]$. For D_2, the correlation lengths are ξ_2 = 5–6 nm throughout the series. Therefore, the pristine solid-state structure is correlated

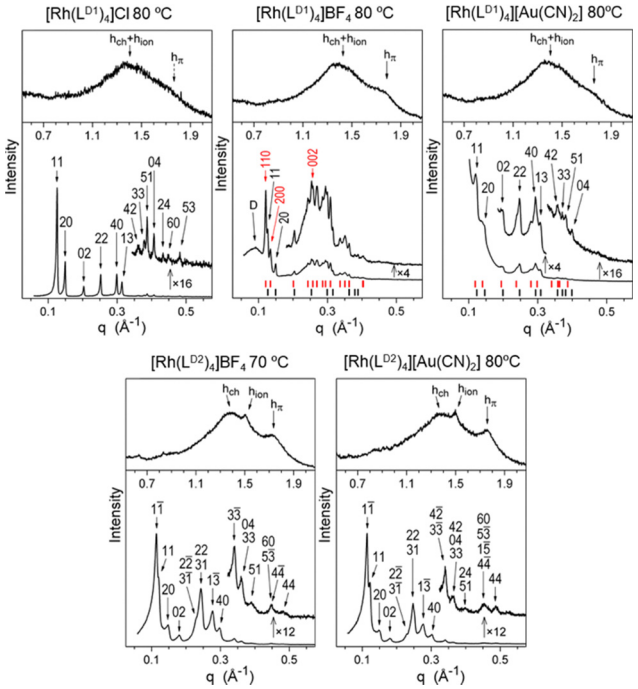

Fig. 6 WAXS/SAXS patterns in the fluid mesophase of [Rh($\mathbf{L^{D1}}$)$_4$](A) (Col$_r$ and Orth) and [Rh($\mathbf{L^{D2}}$)$_4$](A) (Col$_o$) at 80 °C or 70 °C. In red, the signals of the Orth mesophase for the complex [Rh($\mathbf{L^{D1}}$)$_4$](BF$_4$) (**14**), and the Col$_{r2}$ signals for the complex [Rh($\mathbf{L^{D1}}$)$_4$][Au(CN)$_2$] (**19**), both coexisting with a Col$_r$ mesophase, whose signals are shown in black.

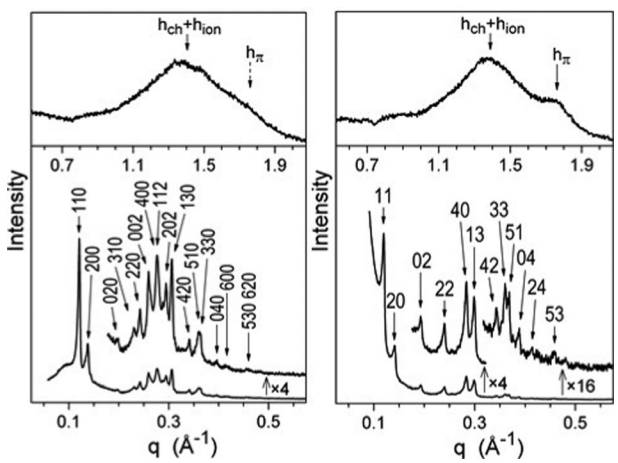

Fig. 7 WAXS (top) and SAXS (bottom) patterns of [Rh($\mathbf{L^{D1}}$)$_4$](BF$_4$) (left) and [Rh($\mathbf{L^{D1}}$)$_4$][Au(CN)$_2$] (right) at 120 °C in the Orth and Col$_{r2}$ mesophases, respectively.

over $\xi/D \approx 3$ neighbouring domains of each type. The slight deviation ξ_1/D = 5–6 for [Rh($\mathbf{L^{D1}}$)$_4$][Au(CN)$_2$] is hard to interpret since the conditions of synthesis might have imprinted an initial thermal history. Furthermore, the scattering signature of triphenylene stacking h_π (expected at *ca.* 3.5 Å) is not separable from scattering contributions of other molecular segments h_{lat}, which indicates irregular pilings. The formation of a superlattice of intermingled domains is however suspected at this early stage by the presence of two intense but broad signals appearing in the small- and mid-angle regions, respectively: a first broad peak, tagged as $D_{Rh/TPh}$, attributed to the average spacing of triphenylenes or organometallic domains separated by chains, and a second, less intense peak, D_{Rh}, from the average spacing of Rh complex domains (Fig. S43, ESI†).

On further heating, in concomitance with the increase of the mesophase fluidity, the complexes rearrange into mesomorphic or pre-organized structures, as revealed by the splitting of the broad scattering into two distinct scattering signals, corresponding respectively to the stacking of TPh cores (h_π) and to the packing of chains and ionic moieties (h_{ch}, h_{ion}), and by the evolution of the two former small-angle scattering signals into better-resolved reflection sets, characteristic of the development of a superlattice. This structuring process was not finished for the [Rh($\mathbf{L^{D1}}$)$_4$](A) compounds at the temperature of SAXS/WAXS measurement and required further heating to 120 °C, contrary to [Rh($\mathbf{L^{D2}}$)$_4$](A) compounds already displaying a small-angle region resolved into sharp reflections (Fig. S47, ESI†).

After annealing the complexes in their high-temperature mesophase or at slightly higher temperatures for 10–15 minutes, temperatures were slowly decreased, and SAXS/WAXS and GIWAXS patterns were recorded at 20 °C in the bulk and in thin films, respectively (Fig. S45 and S46, ESI†). The three compounds of the [Rh($\mathbf{L^{D1}}$)$_4$](A) series display, independently of the anion, a glassy rectangular columnar mesophase (Col$_r$) in the bulk state, characterized by a series of sharp reflections of a large-size two-dimensional rectangular *c*2*mm* lattice (Table S4, ESI†), with $a \approx$ 84–86 Å, and $b \approx$ 62–63 Å) and by the scattering signals from π–π stacking h_π and molten chain packing h_{ch}. In addition, the SAXS/WAXS pattern of [Rh($\mathbf{L^{D1}}$)$_4$](BF$_4$) presents a broad small-angle peak D arising from a local range periodicity, whilst that of [Rh($\mathbf{L^{D1}}$)$_4$][Au(CN)$_2$], a small-angle scattering upturn due to some structural disorder. On the contrary, both [Rh($\mathbf{L^{D2}}$)$_4$](A) compounds lose the long-range order on cooling (compare with Fig. 6) and give amorphous-like states preserving some residual columnar structure correlated over few molecules (short-range ordered oblique lattice Amo$_{Col}$), as revealed by the broadened reflections in the small-angle region and by wide-angle scattering maxima.

The GIWAXS patterns of thin films of all the complexes display well-oriented columnar mesomorphic organizations, with [10] or [11] crystallographic directions aligned onto the film normal (Fig. S46, ESI†). Films of [Rh($\mathbf{L^{D1}}$)$_4$](A) also reveal large superlattices developed to long-range as in the bulk state, but the symmetry is lowered to oblique (Col$_o$). As for the bulk, film states of [Rh($\mathbf{L^{D2}}$)$_4$](A) compounds display oblique superlattices (Col$_o$), but the detailed arrangements are different (see Fig. 9).

Re-heating the samples to 80 °C, the Col$_r$ mesophase formed by the three [Rh($\mathbf{L^{D1}}$)$_4$](A) compounds is identical to the structure frozen in the solid state at 20 °C, and is characterized by a *c*2*mm* superlattice of nearly same size for the three compounds (Fig. 6 and Table S4, ESI†). The piling of TPh units is rather irregular, considering the weak h_π signal, hardly distinguishable from the scattering maxima of the molten chains, h_{ch}, and

ion packing, h_{ion}. Whilst for $[Rh(\mathbf{L^{D1}})_4]Cl$, only one phase is present, for both $[Rh(\mathbf{L^{D1}})_4](BF_4)$ and $[Rh(\mathbf{L^{D1}})_4][Au(CN)_2]$, the Col_r mesophase coexists with another mesophase, likely due to some slow re-organization kinetics (Fig. 6, signals pointed by red labels and position marks; black labels and marks for Col_r). For the complex with the BF_4^- anion, this phase is identified to a three-dimensional orthorhombic mesophase (Orth) and for the other complex with $[Au(CN)_2]^-$, to a second rectangular *c2mm* phase of larger lattice area (Col_{r2}, Table S4, ESI†). Both $[Rh(\mathbf{L^{D2}})_4](A)$ compounds organize into oblique columnar mesophases (Col_o) closed to the one formed in thin films (Fig. 6). Beyond the lattice symmetry change, patterns differ from corresponding $[Rh(\mathbf{L^{D1}})_4](A)$ compounds by the absence of short-range periodicity or scattering upturn in the small-angle region, as well as by the wide-angle region well-resolved into individual h_{ch}, h_{ion} and h_π signals, which indicates a regular arrangement with low degree of structural disorder.

The mesophases of $[Rh(\mathbf{L^{D1}})_4](BF_4)$ and $[Rh(\mathbf{L^{D1}})_4][Au(CN)_2]$ were further investigated at higher temperature, exclusively by SAXS/WAXS since heating *in situ* was not available for GIWAXS experiments. At 120 °C, both complexes are still mesomorphic and display the neat orthorhombic and Col_{r2} phases (Fig. 7), respectively, and the reverse transition to the low-temperature Col_r phase being in both cases observed on cooling. The $a \times b$ sublattice of the Orth phase designs a rectangular *c2mm* lattice of dimensions comparable to the Col_{r2} lattice and substantially larger than the low-temperature Col_r lattices. Apart from the appearance of the three-dimensional superstructure, Orth and Col_{r2} differ by the regularity of the TPh piling, since the h_π scattering is blurred out in the 3D phase and on the contrary amplified relatively to Col_r in the 2D phase.

At 120 °C the complexes $[Rh(\mathbf{L^{D1}})_4](Cl)$, $[Rh(\mathbf{L^{D2}})_4](BF_4)$ and $[Rh(\mathbf{L^{D2}})_4][Au(CN)_2]$ have reached the isotropic liquid state. The eradication of any regular structure is confirmed by the merging of the wide-angle signal into a unique maximum overlapping all lateral distances between molecular segments (h_{lat}, Fig. S47, ESI†). Simultaneously, the D_{Rh} and $D_{Rh/TPh}$ scattering peaks from pristine solid states reappear in the small-angle region, meaning that a columnar superlattice-like organization is maintained at the local range between neighbouring molecules.

Discussion of the self-organization behaviour.

Recall that the two experimental X-ray setups used must be distinguished, which result in some differences in the supramolecular self-assembly: (i) the thin-film configuration (GIWAXS), in which the sample in the mesophase is deposited on a silicon wafer by spin-coating at 20 °C to form a very thin film, and (ii) the bulk configuration (SAXS/WAXS), where the material is maintained in a closed cell. This latter corresponds to the usual method of microscopic observation at variable temperatures.

Independently of the configuration used for the measurements, the large 2D lattice parameters of the mesophases (*a* and *b*, Table S14, ESI†) and the distinct SAXS/WAXS signals, corresponding respectively to the metallic fragment and triphenylene parts, confirmed, in agreement with the detailed crystallographic analysis of reference compounds, that both multiblock $[Rh(\mathbf{L^{D1}})_4](A)$ and $[Rh(\mathbf{L^{D2}})_4](A)$ complexes self-assemble into multi-segregated columnar structures made of differentiated metal-containing piles and triphenylene columns, respectively. Also, whatever the experimental situation, the assembly of the metallic fragment part and counter-ion comes down to a platelet-like "RhA" subunit resembling to a "discotic" mesogen with even piling distance (3.53 Å for RhA in $[Rh(CNXylyl)_4](BF_4)$,[10] close to the normal triphenylene stacking periodicity ($h_\pi \approx 3.5$ Å for TPh), but obviously of different chemical nature. In the single-crystal structure of the compound $[Rh(CNXylyl)_4](BF_4)$, analogue to $[Rh(\mathbf{L^{D2}})_4](BF_4)$ without alkoxytriphenylene substituents, the counter-ions locate in the same plane of the metallic centre and both superimpose (with lateral shift and inversion) to complex and counter-ions of the next molecular layer (Fig. 8, supramolecular model).

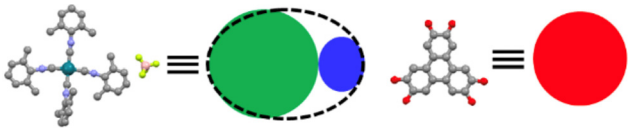

Fig. 8 Left: schematic graphic representation of $[RhL_4](A)$ units. Right: TPh units. The crystal structure of $[Rh(CNXylyl)_4](BF_4)$ is used as real model.[10]

Such structures are effectively obtained throughout both series of complexes with molecular slice thicknesses h_{RhA} (ranging from 3.25 to 3.85 Å, Table S4, ESI†) indicative of RhA arrangements not far from the reference single-crystal. One notable exception is for $[Rh(\mathbf{L^{D2}})_4][Au(CN)_2]$ in film whose substantially higher h_{RhA} value (5.14 Å) is compatible with the intercalation of complex and counter-ion along columns, as in the single-crystal structure of the $Au(CN)_2^-$ reference complex.[10] Intercalation is on the contrary excluded for $[Rh(\mathbf{L^{D1}})_4][Au(CN)_2]$ (h_{RhA} = 3.53 Å), but both $Au(CN)_2$-containing Rh complexes give fluid mesophases at higher temperatures with even lower h_{RhA} values (3.3–3.4 Å). This evolution probably signifies that the intercalated configuration is optimal for the simple ionic systems but that the juxtaposed configuration prevails as it enables a more compact packing of the bulky substituents. Regarding the Tph units, h_π and h_{mol} values are mostly in agreement with those of the solid state, indicating that molecules merely pile into molecular stacks and form the columnar superlattices by intermingling their Tph columns.

As for the arrangements of the two types of columns within the large 2D lattices, let us first examine the thin film situation, at room temperature. In this case, all the compounds form oblique columnar structures (Table S4, ESI†), made of two types of molecular piles per lattice: the Rh complexes and counter-ions superimposed into "RhA" columns (green) occupying the centre of a honeycomb-like sublattice of "TPh" columns (red) separated by molten chains (Fig. 9, chains not represented). In the $[Rh(\mathbf{L^{D1}})_4](A)$ series and in $[Rh(\mathbf{L^{D2}})_4](BF_4)$, counter-ions are located in the periphery of piled complexes and essentially contribute to the cross-sectional area of the columns, piling

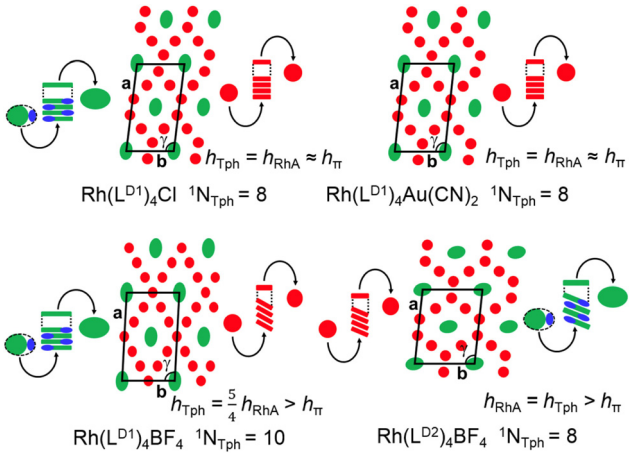

Fig. 9 Schematic views of the supramolecular organizations of $[Rh(\mathbf{L^{D1}})_4](A)$ (A = Cl^-, BF_4^-, $Au(CN)_2^-$) and $[Rh(\mathbf{L^{D2}})_4](BF_4)$ complexes in oblique multicolumnar mesophases (thin film states). The curved arrows help to understand the constitution of the columns, and their projection onto the 2D lattices.

distances of Rh complexes and TPh being similar. The formation of a compact honeycomb thereby requires 8 neighbouring TPh columns with Cl and $[Au(CN)_2]$ anions, in agreement with the 1 : 4 molecular stoichiometry. With BF_4, TPh shares between 10 neighbouring columns, which corollary implies out-of-plane tilting of rings to compensate for their higher intracolumnar spacing. With the more voluminous $\mathbf{L^{D2}}$ ligand, compactness is achieved for the BF_4 complex with 8 neighbouring columns and tilting of both, RhA and TPh. For the $\mathbf{L^{D2}}$ and $Au(CN)_2$ pair (see later), anion and complex intercalate to elongated RhA columns, which is counterbalanced by the reduction of neighbouring TPh to 6 tilted columns.

In different circumstances both stacks may occur inclined in which case the h_{TPh} or h_{RhA} value is different from horizontal stacking. From the variation of these parameters observed in the SAXS/WAXS and GIWAXS studies, the distance between disks in the mesophase and their inclination to the horizontal arrangement can be deduced (Table S4, ESI†).

Fig. 9 shows the distribution of TPh columns and RhA columns vertically viewed in the columnar arrangement and should be understood as not assuming a 1 : 1 ratio between discs because depending on their inclination or not, the distances between discs in a column are not the same. Therefore, while the number N_{TPh} defines the number of columns of TPh per unit cell, in which is contained a column RhA in the centre, and one in each vertex, the ratio of triphenylenes to RhA units must be 4 to 1. Both are related by the different h_{TPh} and h_{RhA} values depending on their inclination.

So, in horizontal stacks in both columns the value of N_{TPh} is 8 and it is met that $h_{TPh} = h_{RhA} \approx 3.5$ Å. This occurs for $[Rh(\mathbf{L^{D1}})_4](Cl)$ (**10**) and $[Rh(\mathbf{L^{D1}})_4][Au(CN)_2]$ (**19**). Obviously, the ratio of red to green columns (8/2 = 4) coincides with the ratio of disks. For $[Rh(\mathbf{L^{D1}})_4](BF_4)$ (**14**) $N_{TPh} = 10$ because the disks of the TPh columns are inclined, the colours only represent the number of columns but not the number of disks as they are separated differently in the green columns and in the red ones. To reach the obligatory ratio of 4 to 1 to which we have alluded, it is necessary that $h_{TPh} = 5/4\ h_{RhA} > h_\pi$.

For the more voluminous $\mathbf{L^{D2}}$ ligand with BF_4 (**15**), both inclined disk stacks are produced with similar inclination with $h_{RhA} = h_{TPh} > h_\pi$ and 8 adjacent TPh columns around a unit of RhA. Such structures are effectively obtained throughout the series with molecular slice thicknesses h_{RhA} (ranging from 3.25 to 3.85 Å) indicative of RhA arrangements not far from the reference single-crystal (Fig. 9 bottom, right).

As hoped for the combination $\mathbf{L^{D2}}$ and $Au(CN)_2$ as anion, Fig. 10) shows the interesting exception of complex $[Rh(\mathbf{L^{D2}})_4][Au(CN)_2]$ (**20**), in which $h_{RhA} = 5.14$ Å is found. This is interpreted as the result of an intercalation of the fragment $Au(CN)_2$ between the disks of the fragment $[Rh(\mathbf{L^{D2}})]$, as depicted in the Fig. 10 left. So, RhA has now another nature, because the $Au(CN)_2$ units (blue spots) are not coplanar with the $[Rh(\mathbf{L^{D2}})]$ units (green circles) but pile up intercalating laterally between rhodium disks. As a consequence, the thickness needed to house one gold plus one rhodium is greater and $h_{RhA} = 4/3h_{TPh} \gg h_\pi$, which produces 6 TPh columns tilted around RhA. The proposal for the RhA green + blue column (Fig. 10, left) can be compared with the crystalline structure observed for the blue polymorph of $[\{L_4Rh\}\{Au(CN)_2\}\{RhL_4\}](Au(CN)_2)$ (Fig. 10, right). In the mesophase the value $h_{RhA} = 5.14$ Å excludes a linear Rh–Au–Rh–Au chain as in the crystal, which requires still larger distances between the $[Rh(\mathbf{L^{D2}})]^+$ units, but is compatible with a rearranged distribution of the Rh centres along the column, with the intrusion of the $Au(CN)_2^-$ fragments in between successive Rh disks, as depicted schematically in Fig. 10, left. This distortion produces a pseudo-zig–zag $(-Rh-Au-Rh-Au-)_\infty$ chain. The "Rh···Rh" sequence could still keep roughly parallel to the column axis, while the Au atoms take randomly helicoidal positions around this Rh···Rh axis. Note that this hypothesis on the arrangement of the metal atoms (which are not observable) in the columns is merely proposed on the basis of geometrical constraints and does not presume anything about the potential presence or lack of Rh···Au intermetallic interactions. Electrostatic or dipolar

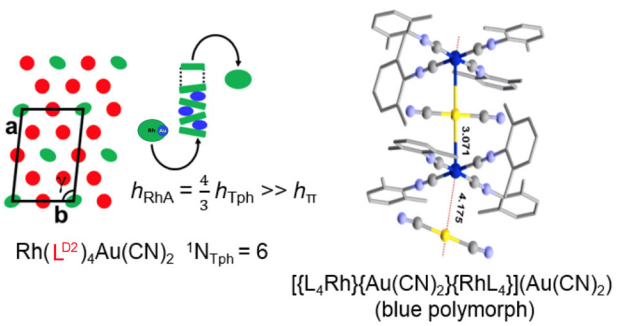

Fig. 10 (Left) Proposed schematic model of molecular self-assembly for complex 20 in thin film state. (Right) Crystal structure of complex $[\{\mathbf{L}_4Rh\}\{Au(CN)_2\}\{Rh\mathbf{L}_4\}](Au(CN)_2)$ (blue polymorph). A zig–zag distorted $(-Rh-Au-Rh-Au-)_\infty$ structure can be imagined from there, as represented in the schematically in the model at left.

Rh/Cl interactions could also provide the attractions needed to compensate the loss of π–π stabilization in the green columns of Fig. 10, left.

In summary, the two complexes containing the dicyanoaurate anion reveal different structural organization within the metallic columns. For **19** (L = $\mathbf{L^{D1}}$), the formation of Rh···Rh···Rh stacking is always found. However, for **20** (L = $\mathbf{L^{D2}}$), an exception is found (only in thin film mesophase at 20 °C): the 2,6-dimethyl substituents in the arylisocyanide weaken the strength of the π–π stacking, and bring to longer Rh···Rh distances,[1d] which facilitates the lateral intercalation of the anion $Au(CN)_2^-$ in the Rh···Rh stacking to produce a pseudo-zig–zag Rh···Au···Rh chain.

In the solid state, all $[Rh(\mathbf{L^{D1}})_4](A)$ compounds show a frozen rectangular columnar mesophase Col_{r1}, with 8 neighbouring TPh columns around RhA, in consistency with the molecular stoichiometry. At higher temperature, the Cl complex early flows to an isotropic liquid state with residual superlattice order. The molecular organizations of the BF_4 and $Au(CN)_2$ congeners, however, rearrange in other fluid mesophases with substantially increased superlattice area and lowered h_{mol}, which reveals redistribution of TPh rings with creation of supplementary columns (Fig. 11).

This process implies that the TPh units are more spaced within columns (larger spacing) and thus introduces a discrepancy with h_π which needs to be compensated either by out-of-plane tilting of rings ($\langle\Psi_{TPh}\rangle > 0$) or by disruption of the columns into segments separated by aliphatic zones ($dh_{TPh,c} > 0$), as previously reported for architectures with single discotic mesogen and overcrowded aliphatic crown.[30] The lattice expansion of the Col_{r2} phase therefore involves the tilting mechanism, while the Orth phase emerges from the 3-dimensional arrangement of segmented columns. The reason of these structural changes is primarily that the fluidizing of the sample at higher temperature effectively enables the redistribution of TPh rings, and presumably that RhA can be compactly surrounded by 10 columns, contrarily to the 8 columns directly obtained from the molecular stoichiometry.

On the other hand, complexes $[Rh(\mathbf{L^{D2}})_4](BF_4)$ and $[Rh(\mathbf{L^{D2}})_4][Au(CN)_2]$ show in the solid state an amorphous undefined superlattice-like order (Amo_{Col}) with a local oblique symmetry. However, both compounds rearrange at higher temperature into fluid oblique columnar mesophases (Col_o) with superlattices of large area corresponding to 10 tilted TPh columns (Fig. 11). The fundamental variation is that the Rh···Au stacking observed for compound **20** in the film situation, is no longer observed in this bulk situation.

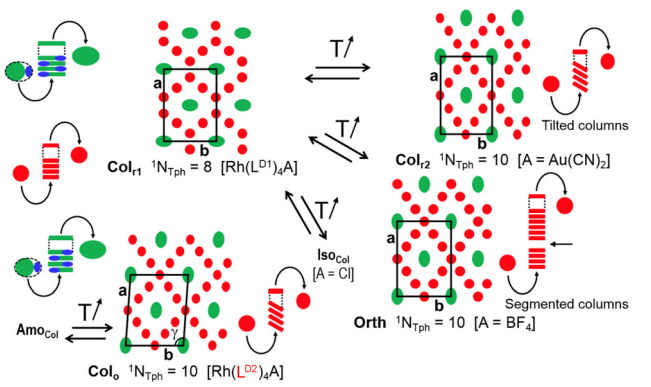

Fig. 11 Schematic views of the molecular self-assembling in the bulk states. All compounds form columnar mesophases with superlattice structures based on RhA columns (green) surrounded by honeycomb-like lattices of Tph columns (red) and spaced by molten chains (not represented); the displayed in-plane orientations are in perfect agreement with the phase symmetry and the optimal space-filling, but are otherwise arbitrary.

Photophysical and electrochemical behaviour in solution

The TPhisocyanide-containing complexes show very weak luminescence in solution, which was not further studied.[2,3b,29–32] The UV-vis absorption spectra of the new ligand $\mathbf{L^{D2}}$ ($\mathbf{L^{D1}}$ was reported in ref. 23*b*) and the complexes **7**–**20** (Scheme 2) were recorded for 10^{-3} M, 10^{-4} M, 5×10^{-5} M and 10^{-5} M solutions in CH_2Cl_2. The data are collected in Table S2 and in Fig. S36–S41 (ESI†). They all show intense bands below 400 nm that, according to the literature,[3a] are associated to intraligand $4dz^2(Rh) \rightarrow 5p$ transitions. Bands around 450–465 nm only appear at high concentrations (10^{-4}–10^{-3}M, indicating that they are associated to $4d\sigma(Rh2) \rightarrow 5p\sigma(Rh2)$/(isocyanide) HOMO/LUMO charge transfer transitions in rhodium dimers. For the complexes with triphenyleneisocyanides, a band at 280 nm, typically associated to the triphenylene group is additionally observed, with the usual extinction coefficients for triphenylene chromophores.[23] Since the spectra are identical for complexes with $(BF_4)^-$ or $[Au(CN)_2]^-$ as anion, and for $\mathbf{L^{D1}}$ or $\mathbf{L^{D2}}$ as ligand, the formation of Rh···Au interactions in 10^{-3} M solutions can be excluded: the formation of oligomers and the associated colours is due to $L_4Rh\cdots RhL_4$ interactions. This is in coincidence with our previous study, where Rh···Au interactions where only formed in the solid state.[10]

Additional support that Rh···Rh association in solution not only occurs for the complexes with small substituents at the isocyanide aryl, but also for the TPhisocyanide complexes, comes from electrochemical studies. Cyclic voltammetry studies were performed for the ligands $\mathbf{L^{D1}}$ and $\mathbf{L^{D2}}$, for complexes **10**, **14**, **19** (with $\mathbf{L^{D1}}$), and for complexes **15** and **20** (with $\mathbf{L^{D2}}$ on dilute (5×10^{-5}M) and concentrated (10^{-3}M) CH_2Cl_2 solutions with tetra-*n*-butylammonium hexafluorophosphate (0.1 M)). Complete data of electrochemical parameters and HOMO/LUMO energy levels are given in Table S6 and in Fig. S51–S62 (ESI†).

All the compounds, except the free ligands $\mathbf{L^{D1}}$ and $\mathbf{L^{D2}}$ and complex **10** (10^{-3}M), show irreversible oxidation processes. In dilute solutions the complexes give an intense peak in the range 0.89–1.05 eV. This oxidation peak appears also in the solutions of both ligands and therefore it corresponds to the energy of the HOMO orbital for the TPh fragment.[33] The case of $[Rh(\mathbf{L^{D1}})_4][Au(CN)_2]$ (Fig. 12) is representative of the general behaviour of the complexes and shows how the reversible voltammogram of the monomeric complex at the lower concentration is intruded at higher concentration by the participation of oligomeric species with Rh···Rh interactions.

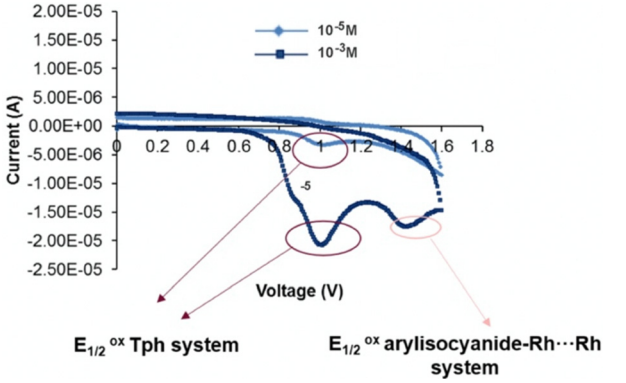

Fig. 12 Cyclic voltammogram of $[Rh(\mathbf{L^{D1}})_4][Au(CN)_2]$ (**19**) in CH_2Cl_2 at two molar concentrations.

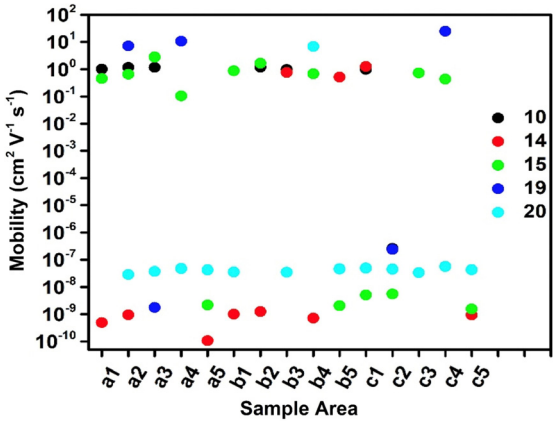

Fig. 13 Hole mobilities measured, after thermal treatment, in compounds **10**, **14**, **19**, **15** and **20**. Different areas of each sample are labelled with letters and numbers, as described in the ESI.†

Additionally, a second oxidation peak, in the range 1.27–1.60 eV, appears only in the concentrated solutions of the complexes. Since this oxidation peak is always observed, independent of the anion, it is assigned to the HOMO energy of the oligomeric $Rh^{I}\cdots Rh^{I}$ species in solution.

Overall, the photophysical and cyclic voltammetry data in CH_2Cl_2 solution confirm the molecular association and formation of Rh···Rh interactions at molar concentrations above 10^{-4}. Moreover, they also support the absence of Rh···Au interactions in solution when $[Au(CN)_2]^-$ is present as counteranion.

Hole mobility studies

The HOMO energy levels of the complexes determined in the voltamperometric studies are suitable for charge injection from gold electrodes, which opens the possibility for the experimental hole mobility study of compounds **10**, **14**, **19**, **15** and **20**. Hole mobilities were measured using the Space Charge Limited Current (SCLC) method, on samples approximately 10 μm thick. Details of sample preparation and measurements can be found in the ESI.†

The SCLC mobility reflects the average mobility across the entire thickness of the sample. In anisotropic media, *e.g.* in columnar mesophases, it significantly depends on the alignment of the columns: it will be higher the more uniformly and macroscopically oriented the columns are along the direction of displacement of the charges. The result for of the measurements on complexes **10**, **14**, **19**, **15** and **20** are shown in Fig. 13.

Usually the columnar units do not spontaneously align in the direction of the applied electric field, so it is necessary to use thermal treatments, or other means, to induce the preferred alignment. In the case of complexes **10**, **14**, **19**, **15** and **20**, POM showed, before any thermal treatment, an uneven distribution of the mesophase director and, consequently, mobility values in the order of 10^{-8}–10^{-9} $cm^2\ V^{-1}\ s^{-1}$ were measured for all complexes. After the thermal treatments described in the ESI,† although a clear change in the orientation of the columns was not observed by POM, in some areas of most samples it was possible to measure a much higher charge mobility. This may be due to the fact that, although the thermal treatment failed to induce a dominant favourable homogeneous orientation throughout the samples, due to the high viscosity of the materials, this orientation was still achieved in some areas.

This "binary" distribution of the measured mobility values after thermal treatments, where the two ranges of measured mobility are separated by 7–9 orders of magnitude, was observed for all samples of all complexes. No intermediate value of mobility was ever recorded. Attributing the very low mobility measured in some sample areas to poor or unfavourable orientation order, such measurements were neglected and charge mobility for each complex was obtained by averaging only the values within the high mobility range. These average results are listed in Table 2.

The experimental values of charge mobility often depend on the measurement technique and experimental conditions. As a consequence, the values reported in Table 2 should be valid for comparison of order of magnitude with literature values.[34] Yet, since the same experimental conditions were always used, direct comparison among the results for the five semiconductor complexes in the Table is also valid. The columnar mesophases of this study show a much higher charge mobility than the values recorded and reported in mesophases formed by triphenylene columns only, usually in the 10^{-4}–10^{-2} $cm^2\ V^{-1}\ s^{-1}$ range.[15] This indicates that columns formed by the metal-anion pair play a very important role in determining the charge mobility values of the studied complexes. The same behaviour was reported also in mesophases formed by triphenylene-metal complexes with respect to mesophases formed by triphenylene

Table 2 Average measured for hole mobility ($cm^2\ V^{-1}\ s^{-1}$)

Complex	Mobility
$[Rh(\mathbf{L^{D1}})_4](Cl)$ (**10**)	1 ± 0.4
$[Rh(\mathbf{L^{D1}})_4](BF_4)$ (**14**)	0.9 ± 0.6
$[Rh(\mathbf{L^{D1}})_4][\mathbf{Au(CN)_2}]$ (**19**)	14 ± 0.5
$[Rh(\mathbf{L^{D2}})_4](BF_4)$ (**15**)	0,9 ± 0.7
$[Rh(\mathbf{L^{D2}})_4][\mathbf{Au(CN)_2}]$ (**20**)	8 ± 0.1[a]

[a] This datum refers to a single sample area.

only, both in the case in which the triphenylene columns are segregated with respect to the columns formed by the metal,[23d,23f] and in the case in which they are not.[35] It is also possible to note a dependence of charge mobility on the nature of the anion: with $[Au(CN)_2]^-$ the mobility is one order of magnitude higher than with $(BF_4)^-$ or Cl^-. Since this occurs identically for the $\mathbf{L^{D1}}$ and for the $\mathbf{L^{D2}}$ complexes, and since the strict conditions under which Rh···Au intercalation occurs (thin films at 20 °C) most probably exclude its presence in the samples used for the measurement of hole mobility, this phenomenon is more likely associated to the presence of non-intercalated columns of the ionic pairs $[Rh(\mathbf{L^{D1}})_4](Au(CN)_2)$ or $[Rh(\mathbf{L^{D2}})_4](Au(CN)_2)$, as shown in Fig. 9. Some contribution of Au···Au interactions of the $[Au(CN)_2]^-$ anions in these discotic $[RhL_4][Au(CN)_2]$ might explain this extra hole mobility, but we cannot provide any experimental support for this hypothesis.

Conclusions

Two families of mesogenic complexes with triphenyleneisocyanides, $[Rh(\mathbf{L})_4](A)$ ($L = \mathbf{L^{D1}}$ or $\mathbf{L^{D2}}$; $A^- = Cl^-$, $(BF_4)^-$ or $Au(CN)_2^-$) have been prepared and their properties studied. All members of both families generate mesophases with multicolumnar structures containing two types of columns: those formed by π–π stacking of triphenylenes, and those resulting from π–π stacking of the organometallic $[Rh^I(CNAr)_4]^+$ units, both being connected by a hexamethylene spacer. Several 2D mesophases with different symmetries and columnar arrangements (Col_r, Col_o) and a 3D mesophase (Orth) are observed in these molecular systems. The structural features of the mesophases are conditioned by the isocyanide substituents, the type of anion used, and the conditions and temperature of the experiments carried out. These conditions result in compensating inclinations between the TPh disks and the RhA units that drive and define the network symmetry found in the mesophases.

For the ligand $\mathbf{L^{D1}}$, with no or small tilting of the aryls relative to the RhC_4 square plane, the four isocyanide ligands can strongly cooperate in the intra-unit π–π stacking, thus overcoming the cation–cation repulsions and giving rise to polymeric column formation with Rh···Rh interactions. These interactions lead to mesophases with deep green colours and large mesogenic intervals (from –9 to 169 °C).

The presence of two *ortho*-substituents in the aryl of $\mathbf{L^{D2}}$, which force larger tilting of the aryls that hampers achieving the best π–π aryl stacking, the blue colours and the similarity in columnar parameters with the $\mathbf{L^{D1}}$ complexes still support polymeric Rh···Rh interactions with clearly shorter but still large mesogenic intervals (from –8 to 89 °C). There is only one exception to this structural behaviour in the mesophases of the complexes with $\mathbf{L^{D2}}$: with $[Au(CN)_2]^-$ as counter-anion, and only in thin films at 20 °C, the substantially higher value of h_{RhA} (5.14 Å, compared to a 3.4–3.55 Å range for the rest of the mesophases) is compatible with the intercalation of the Rh cationic complex and the Au counter-ion along columns to give a zig–zag Rh–Au–Rh–Au helicoidal atomic arrangement with anion–cation attractions compensating the loss of the relatively inefficient π–π aryl stacking of this structure, as found previously in the related single-crystal structure of complex $[\{\mathbf{L}_4Rh\}\{Au(CN)_2\}\{Rh\mathbf{L}_4\}](Au(CN)_2)$ (blue polymorph).[10] This produces elongated RhA columns, which is counterbalanced by the reduction of neighbouring TPh to 6 tilted columns. The structurally singular zig–zag Rh–Au–Rh–Au organization in this mesophase with $\mathbf{L^{D2}}$ does not prevail at higher temperatures and evolves to a Col_o deep blue mesophase with $Rh^I\cdots Rh^I$ interactions, a more expanded symmetry, and the anion arranged in the same plane as the cationic unit $[Rh\mathbf{L}_4]^+$.

Thus, with this exception, all the mesophases of the complexes with $\mathbf{L^{D1}}$ or $\mathbf{L^{D2}}$ maintain polymeric π–π aryl stacking and Rh···Rh interactions (at somewhat different distances for the two ligands). It is remarkable that in all this complex scaffolding with plenty of π–π stacking of triphenylenes and a large aliphatic continuum, an apparently small detail such as the absence or presence of two Me groups in the isocyanide aryl is decisive for the clearing temperatures and the mesophase ranges of the resulting material, supporting the importance of the π–π stacking of the isocyanide aryls in the Rh complex for the stabilization of whole mesophase building. In contrast with the first pictorial impression in our mesophase illustrations (many red circles of TPh and fewer green circles of RhL_4A) it is the latter the ones that support the formation of this segregated columnar alignment.

The hole mobility of the complexes is two to four orders of magnitude higher than those reported for columnar mesophases formed by triphenylene derivatives only, demonstrating again importance of the columns formed by the metal-containing units. The mobilities measured in the mesophases containing $[Au(CN)_2]^-$ are still one order of magnitude higher than those recorded in the mesophases containing Cl^- or BF_4^-.

Author contributions

The manuscript has been written through contributions of all authors, who have given approval to this final version of the manuscript. V. Conejo-Rodríguez is author of the synthesis and full characterization of all the ligands and complexes, including molecular characterization, DSC and POM studies, and photophysical and electrochemical studies in solution. B. Donnio and B. Heinrich are responsible of the SAXS/WAXS and GIWAXS studies; R. Termine and A. Golemme have contributed the hole mobility studies; P. Espinet is responsible of the organization and coordination of the work and the final writing of the publication.

Conflicts of interest

There are no conflicts to declare.

Acknowledgements

We thank the Spanish MICINN (Project PID2020-118547GB-I00) for financial support, and Dr Marconi N. Peñas-Defrutos for

resolution of the X-ray diffraction structures. V. C.-R. thanks MINECO for a predoctoral FPI studentship. B.D. and B.H. thank CNRS and the University of Strasbourg for support and Pohang Accelerator Laboratory (PAL) for giving us the opportunity to perform the GIWAXS measurements, MEST and POSTECH for supporting these experiments, Dr Hyungju Ahn for adjustments and help, and other colleagues from the 9A USAXS beamline for assistance. R.T. and A.G. thank the Italian Ministry of University and Research for a ''Progetto STAR 2'' (PIR01_00008) and to Franco Cofone of NANOTEC-CNR for helping in samples preparation.

References

1 (*a*) J. W. Dart, M. K. Lloyd, R. Mason and J. A. McCleverty, *J. Chem. Soc., Dalton Trans.*, 1973, 2039; (*b*) D. Baumann, H. J. Kellek, D. Nöthe, H. H. Rupp and G. Uhlman, *Z. Naturforsch., B: Anorg. Chem., Org. Chem.*, 1976, **31B**, 912; (*c*) K. R. Mann, N. S. Lewis, R. M. Williams, H. B.Gray and J. G. Gordon, *Inorg. Chem.*, 1978, **17**, 828; (*d*) Y. Yamamoto,, K. I. Aoki and H. Yamazaki, *Inorg. Chem.*, 1979, **18**, 1681; (*e*) H. Endres, N. Gottstein, H. J. Keller, R. Martin, W. Rodemer and W. Steiger, *Z. Naturforsch., B: Anorg. Chem., Org. Chem.*, 1979, **34B**, 827; (*f*) K. R. Mann, J. A. Thich, R. A. Bell, C. L. Coyle and H. B. Gray, *Inorg. Chem.*, 1980, **19**, 2462; (*g*) S. Miya, Y. Yamamoto and H. Yamazaki, *Inorg. Chem.*, 1982, **21**, 1486; (*h*) Y. Yamamoto, Y. Wakatsuki and H. J. Yamazaki, *Organometallics*, 1983, **2**, 1604.

2 S. Grimme and J.-P. Djukic, *Inorg. Chem.*, 2011, **50**, 2619.

3 (*a*) V. W.-W. Yam, V. K.-M. Au and S. Y.-L. Leung, *Chem. Rev.*, 2015, **115**, 7589; (*b*) A. K.-W. Chan, K. M.-C. Wong and V. W.-W. Yam, *J. Am. Chem. Soc.*, 2015, **137**, 6920.

4 Y. Chen, K. Li, H. O. Lloyd, W. Lu, S. S.-Y. Chui and C.-M. Che, *Angew. Chem., Int. Ed.*, 2010, **49**, 9968.

5 T. Tominaga and T. Mochida, *Chem. – Eur. J.*, 2018, **24**, 6239.

6 H. Ito, T. Kato and M. Sawamura, *Chem. – Asian J.*, 2007, **2**, 1436.

7 (*a*) G. Cui, X.-Y. Cao, W.-H. Fang, M. Dolg and W. Thiel, *Angew. Chem., Int. Ed.*, 2013, **52**, 10281; (*b*) M. Iwamura, K. Nozaki, S. Takeuchi and T. Tahara, *J. Am. Chem. Soc.*, 2013, **135**, 538; (*c*) S. R. Hettiarachchi, M. A. Rawashdeh-Omary, S. M. Kanan, M. A. Omary, H. H. Patterson and C. P. Tripp, *J. Phys. Chem. B*, 2002, **106**, 10058; (*d*) M. A. Rawashdeh-Omary, M. A. Omary, H. H. Patterson and J. P. Fackler, *J. Am. Chem. Soc.*, 2001, **123**, 11237; (*e*) M. A. Rawashdeh-Omary, M. A. Omary and H. H. Patterson, *J. Am. Chem. Soc.*, 2000, **122**, 10371.

8 (*a*) Q. Liu, M. Xie, X. Chang, Q. Gao, Y. Chen and W. Lu, *Chem. Commun.*, 2018, **54**, 12844; (*b*) Q. Liu, M. Xie, X. Chang, S. Cao, C. Zou, W.-F. Fu, C.-M. Che, Y. Chen and W. Lu, *Angew. Chem., Int. Ed.*, 2018, **57**, 6279.

9 M. Barcenilla, C. L. Folcia, J. Ortega, J. Etxebarria, S. Coco and P. Espinet, *J. Mater. Chem. C*, 2022, **10**, 932.

10 V. Conejo-Rodríguez, M. N. Peñas–Defrutos and P. Espinet, *Chem. Commun.*, 2019, **55**, 5005.

11 Reviews in journals: (*a*) P. Espinet, M. A. Esteruelas, L. Oro, J. L. Serrano and E. Sola, *Coord. Chem. Rev.*, 1992, **117**, 215; (*b*) B. Donnio, *Inorg. Chim. Acta*, 2014, **409**, 53.

12 Books and book chapters: (*a*) *Metallomesogens*, ed. J. L. Serrano, VCH, Weinheim, Germany, 1996; (*b*) D. W. Bruce, *Inorganic Materials*, ed. D. W. Bruce, D. O'Hare, Wiley, Chichester, U.K, 2nd edn, 1996, Ch. 8; (*c*) B. Donnio, D. Guillon, D. W. Bruce and R. Deschenaux, (Applications III: Functional Materials, Environmental and Biological Applications), *Metallomesogens, in Comprehensive Organometallic Chemistry III: From Fundamentals to Applications*, ed. Crabtree, R. H., Mingos, D. M. P., Elsevier, Oxford, U.K, 2006, ch. 12.05, vol. 12, pp. 195–294; (*d*) S. Coco and P. Espinet, in Liquid Crystals Based on Gold Compounds, *Gold Chemistry: Applications and Future Directions in the Life Sciences*, ed. Mohr, F., Wiley-VCH Verlag GmbH & CoKGaA, Weiheim, Germany, 2009, pp. 357–396.

13 S. Sergeyev, W. Pisula and Y. H. Geerts, *Chem. Soc. Rev.*, 2007, **36**, 1902.

14 (*a*) Y. Shimizu, A. Kurobe, H. Monobe, N. Terasawa, K. Kiyohara and K. Uchida, *Chem. Commun.*, 2003, 1676; (*b*) R. J. Bushby, N. Boden, C. A. Kilner, O. R. Lozman, Z. Lu, Q. Liu and M. A. Thornton-Pett, *J. Mater. Chem.*, 2003, **13**, 470; (*c*) T. Kato, N. Mizoshita and K. Kishimoto, *Angew. Chem., Int. Ed.*, 2006, **45**, 38; (*d*) S. Kumar, *Chem. Soc. Rev.*, 2006, **35**, 83; (*e*) S. K. Gupta, V. Raghunathan and S. Kumar, *New. J. Chem.*, 2008, **33**, 112; (*f*) H. K. Bisoyi and S. Kumar, *Tetrahedron Lett.*, 2008, **49**, 3628; (*g*) X. Feng, V. Marcon, W. Pisula, M. R. Hansen, J. Kirkpatrick, F. Grozema, D. Andrienko, K. Kremer and K. Müllen, *Nat. Mater.*, 2009, **8**, 421; (*h*) I. Tahar-Djebbar, F. Nekelson, B. Heinrich, B. Donnio, D. Guillon, D. Kreher, F. Mathevet and A.-J. Attias, *Chem. Mater.*, 2011, **23**, 4653; (*i*) S. Sauer, N. Steinke, A. Baro, S. Laschat, F. Giesselmann and W. Kantlehner, *Chem. Mater.*, 2008, **20**, 1909.

15 T. Wöhrle, I. Wurzbach, J. Kirres, A. Kostidou, N. Kapernaum, J. Litterscheidt, J. C. Haenle, P. Staffeld, A. Baro, F. K. Giesselmann and S. Laschat, *Chem. Rev.*, 2016, **116**, 1139.

16 (*a*) C. Tschierske, *Angew. Chem., Int. Ed.*, 2013, **52**, 8828; (*b*) R. C. Borner, R. J. Bushby, A. N. Cammidge and M. V. Jesudason, *Liq. Cryst.*, 2006, **33**, 1439; (*c*) X. Kong, Z. He, H. Gopee, X. Jing and A. N. Cammidge, *Tetrahedron Lett.*, 2011, **52**, 77; (*d*) S. K. Varshney, *Liq. Cryst.*, 2013, **40**, 1477.

17 (*a*) S. Kumar, *Liq. Cryst.*, 2004, **31**, 1037; (*b*) S. Kumar, *Liq. Cryst.*, 2005, **32**, 1089.

18 (*a*) W. Pisula and K. Müllen, *Discotic Liquid Crystals as Organic Semiconductors. In Handbook of Liquid Crystals*, ed. J. W. Goodby, P. J. Collings, T. Kato, C. Tschierske, H. F. Gleeson and P. Raynes, Wiley-VCH, Weinheim, 2014, vol. 8, p. 627; (*b*) D. Sonet and B. Bibal, *Tetrahedron Lett.*, 2019, **60**, 872.

19 (*a*) W. Pisula, M. Kastler, D. Wasserfallen, M. Mondeshki, J. Piris, I. Schnell and K. Müllen, *Chem. Mater.*, 2006, **18**, 3634; (*b*) M. O'Neill and S. M. Kelly, *Adv. Mater.*, 2003, **15**, 1135; (*c*) J. Simmerer, B. Glüsen, W. Paulus, A. Kettnwe,

P. Schuhmacher, A. Adam, K. H. Etzbach, K. Siemensmeyer, J. H. Wendorff, P. Roisin, G. P. Rigby, R. Nolte, M. J. Cook and S. C. Thorpe, *Sens. Actuators B*, 1993, **13–14**, 276; (*d*) D. Adam, P. Schuhmacher, J. Simmerer, L. Haussling, K. Siemensmeyer, K. H. Etzbach, H. Ringsdorf and D. Haarer, *Nature*, 1994, **371**, 141.

20 (*a*) B. Mohr, G. Wegner and K. Ohta, *Chem. Comm.*, 1995, 995; (*b*) J. L. Schulte, S. Laschat, R. Schulte-Ladbeck, V. von Arnim, A. Schneider and H. Finkelmann, *J. Organomet. Chem.*, 1998, **552**, 171.

21 (*a*) S. Kumar and S. K. A. Varshney, *Liq. Cryst.*, 2001, **28**, 161; (*b*) A. N. Cammidge and H. Gopee, *Chem. Commun.*, 2002, 966.

22 (*a*) Y. Wang, Y. Liu, J. Luo, H. Qi, X. Li, M. Nin, M. Liu, D. Shi, W. Zhu and Y. Cao, *Dalton Trans.*, 2011, **40**, 5046; (*b*) F. Bai, X. Yang, H. Guo and C. Li, *Tetrahedron Lett.*, 2013, **54**, 409; (*c*) J. Shi, Y. Wang, M. Xiao, P. Zhong, Y. Liu, H. Tan, M. Zhu and W. Zhu, *Tetrahedron.*, 2015, **71**, 463.

23 (*a*) E. Tritto, R. Chico, G. Sanz-Enguita, C. L. Folcia, J. Ortega, S. Coco and P. Espinet, *Inorg. Chem.*, 2014, **53**, 3449; (*b*) E. Tritto, R. Chico, J. Ortega, C. L. Folcia, J. Etxebarria, S. Coco and P. Espinet, *J. Mater. Chem. C*, 2015, **3**, 9385; (*c*) R. Chico, C. Domínguez, B. Donnio, B. Heinrich, S. Coco and P. Espinet, *Cryst. Growth Des.*, 2016, **16**, 6984; (*d*) R. Chico, E. de Domingo, C. Domínguez, B. Donnio, B. Heinrich, R. Termine, A. Golemme, S. Coco and P. Espinet, *Chem. Mater.*, 2017, **29**, 7587–7595; (*e*) A. B. Miguel−Coello, M. Bardají, S. Coco, B. Donnio, B. Heinrich and P. Espinet, *Inorg. Chem.*, 2018, **57**(8), 4359; (*f*) E. Domingo, C. L. Folcia, J. Ortega, J. Etxebarria, R. Termine, A. Golemme, S. Coco and P. Espinet, *Inorg, Chem.*, 2020, **59**, 10482.

24 (*a*) I. Ugi and R. Meyr, *Chem. Ber./Recl.*, 1960, **93**, 239; (*b*) W. P. Weber, G. W. Gokel and I. Ugi, *Angew. Chem., Int. Ed. Engl.*, 1972, **11**, 530.

25 T. V. Ashworth, D. C. Liles, H. E. Oosthuizen and E. Singleton, *Acta Cryst.*, 1984, **C40**, 1169.

26 For concepts associated to non-covalent interactions (NCI) see: R. F. W. Bader, *Atoms in Molecules: A Quantum Theory*, Oxford University Press, Oxford, U.K, 1990.

27 S. Alvarez, *Dalton Trans.*, 2013, **42**, 8617.

28 B. Cordero, V. Gómez, A. E. Platero-Prats, M. Revés, J. Echeverría, E. Cremades, F. Barragán and S. Alvarez, *Dalton Trans.*, 2008, 2832.

29 (*a*) K.-Q. Zhao, X.-Y. Bai, B. Xiao, Y. Gao, P. Hu, B.-Q. Wang, Q.-D. Zeng, C. Wang, B. Heinrich and B. Donnio, *J. Mater. Chem. C*, 2015, **3**, 11735; (*b*) W. Zhang, W.-H. Yu, C. Feng, S.-K. Xiang, B.-Q. Wang, K.-Q. Zhao, H.-L. Ni and P. Hu, *Liq. Cryst.*, 2020, **47**, 1100; (*c*) A. Herbaut and E. Baranoff, *Chimia*, 2015, **69**, 520.

30 (*a*) N. S. Lewis, K. R. Mann, J. G. Gordon and H. B. Gray, *J. Am. Chem. Soc.*, 1976, **98**, 7461; (*b*) A. Efraty, I. Feinstein, F. Frolow and L. Wackerle, *J. Am. Chem. Soc.*, 1980, **102**, 6343; (*c*) M. L. Winzenburg, J. A. Kargol and R. J. Angelici, *J. Organomet. Chem.*, 1983, **249**, 415; (*d*) A. L. Balch and M. M. Olmstead, *J. Am. Chem. Soc.*, 1976, **98**, 2354.

31 (*a*) K. R. Mann, J. G. Gordon and H. B. Gray, *J. Am. Chem. Soc.*, 1975, **97**, 3553; (*b*) B. E. Bursten and R. F. Fenske, *Inorg. Chem.*, 1977, **16**, 963.

32 D. Myśliwiec, B. Donnio, P. J. Chmielewski, B. Heinrich and M. Stępień, *J. Am. Chem. Soc.*, 2012, **134**, 4822.

33 (*a*) M. M. Ahmida and S. H. Eichhorn, *ECTS Trans.*, 2010, **25**, 1; (*b*) S. J. Mahoney, M. M. Ahmida, H. Kayal, N. Fox, Y. Shimizucand and S. H. Eichhor, *J. Mater. Chem.*, 2009, **19**, 9221.

34 R. Termine and A. Golemme, *Int. J. Mol. Sci.*, 2021, **22**, 877.

35 B. Feringan, R. Termine, A. Golemme, J. M. Granadino-Roldán, A. Navarro, R. Giménez and T. Sierra, *J. Mater. Chem. C*, 2021, **9**, 1972.